Translational Cancer Mechanisms and Therapy

Clinical Cancer Research

Elective Nodal Irradiation Attenuates the Combinatorial Efficacy of Stereotactic Radiation Therapy and Immunotherapy

Ariel E. Marciscano[1], Ali Ghasemzadeh[2], Thomas R. Nirschl[2], Debebe Theodros[2], Christina M. Kochel[2], Brian J. Francica[2], Yuki Muroyama[2], Robert A. Anders[2,3], Andrew B. Sharabi[4], Esteban Velarde[1], Wendy Mao[2], Kunal R. Chaudhary[5], Matthew G. Chaimowitz[6], John Wong[1], Mark J. Selby[7], Kent B. Thudium[7], Alan J. Korman[7], David Ulmert[8], Daniel L.J. Thorek[2,9], Theodore L. DeWeese[1,2], and Charles G. Drake[2,6]

Abstract

Purpose: In the proper context, radiotherapy can promote antitumor immunity. It is unknown if elective nodal irradiation (ENI), a strategy that irradiates tumor-associated draining lymph nodes (DLN), affects adaptive immune responses and combinatorial efficacy of radiotherapy with immune checkpoint blockade (ICB).

Experimental Design: We developed a preclinical model to compare stereotactic radiotherapy (Tumor RT) with or without ENI to examine immunologic differences between radiotherapy techniques that spare or irradiate the DLN.

Results: Tumor RT was associated with upregulation of an intratumoral T-cell chemoattractant chemokine signature (CXCR3, CCR5-related) that resulted in robust infiltration of antigen-specific $CD8^+$ effector T cells as well as $FoxP3^+$ regulatory T cells (Tregs). The addition of ENI attenuated chemokine expression, restrained immune infiltration, and adversely affected survival when combined with ICB, especially with anti-CLTA4 therapy. The combination of stereotactic radiotherapy and ICB led to long-term survival in a subset of mice and was associated with favorable CD8 effector-to-Treg ratios and increased intratumoral density of antigen-specific $CD8^+$ T cells. Although radiotherapy technique (Tumor RT vs. ENI) affected initial tumor control and survival, the ability to reject tumor upon rechallenge was partially dependent upon the mechanism of action of ICB; as radiotherapy/anti-CTLA4 was superior to radiotherapy/anti-PD-1.

Conclusions: Our results highlight that irradiation of the DLN restrains adaptive immune responses through altered chemokine expression and $CD8^+$ T-cell trafficking. These data have implications for combining radiotherapy and ICB, long-term survival, and induction of immunologic memory. Clinically, the immunomodulatory effect of the radiotherapy strategy should be considered when combining stereotactic radiotherapy with immunotherapy. *Clin Cancer Res; 24(20); 5058–71. ©2018 AACR.*

Introduction

Ionizing radiation is a cytotoxic therapy that primarily exerts its therapeutic effect via induction of double-stranded DNA breaks in tumor cells. Recent studies linking DNA damage with radiation-mediated immunogenicity provided mechanistic evidence that the immunomodulatory properties of radiotherapy also contribute to its therapeutic efficacy (1–3). Within the irradiated tumor microenvironment (TME), radiotherapy initiates a cascade of molecular and cellular events leading to immunogenic cell death, upregulation of MHC class I, enhanced type I IFN signaling and dendritic cell activation (4–7). Ultimately, effective antitumor adaptive immunity requires the priming and subsequent chemokine-driven trafficking of tumor-specific $CD8^+$ CTLs into the TME to mediate tumoricidal effector functions (8–10).

The tumor-associated draining lymph node (DLN) is essential to the generation of tumor-specific $CD8^+$ effector T cells given that

[1]Department of Radiation Oncology & Molecular Radiation Sciences, Sidney Kimmel Comprehensive Cancer Center, Johns Hopkins University School of Medicine, Baltimore, Maryland. [2]Department of Oncology, Sidney Kimmel Comprehensive Cancer Center, Johns Hopkins University School of Medicine, Baltimore, Maryland. [3]Department of Pathology, Sidney Kimmel Comprehensive Cancer Center, Johns Hopkins University School of Medicine, Baltimore, Maryland. [4]Department of Radiation Medicine and Applied Sciences, University of California, San Diego, Moores Cancer Center, San Diego, California. [5]Department of Radiation Oncology, Columbia University Medical Center, New York, New York. [6]Division of Hematology and Oncology, Herbert Irving Comprehensive Cancer Center, Columbia University Medical Center, New York, New York. [7]Bristol-Myers Squibb Company, Redwood City, California. [8]Molecular Pharmacology Program, Memorial Sloan Kettering Cancer Center, New York, New York. [9]Division of Nuclear Medicine and Molecular Imaging, Department of Radiology and Radiological Science, Johns Hopkins University School of Medicine, Baltimore, Maryland.

Note: Supplementary data for this article are available at Clinical Cancer Research Online (http://clincancerres.aacrjournals.org/).

Current address for C.M. Kochel: Tizona Therapeutics, South San Francisco, California; and current address for B.J. Francica, Aduro Biotech Inc., Berkeley, California.

Corresponding Author: Charles G. Drake, Division of Hematology/Oncology, Columbia University Medical Center, Herbert Irving Comprehensive Cancer Center, 177 Fort Washington Avenue, Suite 6GN-435, New York, NY 10032. Phone: 212-305-2055; Fax: 212-305-3035: E-mail: cgd2139@cumc.columbia.edu

doi: 10.1158/1078-0432.CCR-17-3427

AACR

Translational Relevance

As the combination of immunotherapy with radiotherapy gains clinical traction, an improved understanding of mechanisms of potential synergy is important to maximize benefit. The practice of irradiating the tumor-associated draining lymph nodes (DLN), known as elective nodal irradiation (ENI), is frequently used by radiation oncologists when treating localized cancers to address potential subclinical nodal disease. It remains unknown whether irradiation of the DLN affects combinatorial efficacy with immune checkpoint blockade (ICB). These studies show that ENI restrains the potent adaptive antitumor immunity that can be achieved by combining stereotactic tumor-directed radiotherapy and ICB. Mechanistically, ENI modulated chemokine signaling, leading to reduced immune infiltration as well as to an unfavorable balance between tumoricidal and immunosuppressive intratumoral immune cells (reflected in a decreased CD8 effector-to-Treg ratio). Exclusion of the DLN from the radiotherapy target volume should be examined in future clinical trials to promote synergy between ICB and radiotherapy.

it is one of the main locations at which dendritic cells prime antigen-specific $CD8^+$ T cells (7, 11–13). Takeshima and colleagues observed that the DLN is indispensable for radiation-induced accumulation of antigen-specific intratumoral CTL, as DLN-deficient mice and mice with surgically ablated DLN showed a significant reduction in tumor control following radiotherapy (14). Similarly, we demonstrated that stereotactic radiotherapy enhances cross-presentation of MHC class I–restricted tumor-associated antigens in the DLN as the major mechanism by which radiotherapy promotes antigen-specific immune responses and synergizes with immunotherapy (15).

It is currently unknown whether irradiation of the DLN augments or restrains adaptive immune responses and impacts potential combinatorial efficacy with immune checkpoint blockade (ICB). This question carries significant clinical relevance as the strategy of elective nodal irradiation (ENI) is a commonly employed in the practice of radiation oncology, although its role is controversial or under investigation in certain cancer subtypes (16–19). ENI involves radiotherapy delivered to the primary tumor as well as the irradiation of clinically uninvolved regional lymph nodes in the setting of a localized cancer to address potential nodal micrometastases. As technology evolved over the past decades, stereotactic radiotherapy is currently able to deliver precise and conformal high-dose radiation while either sparing or targeting the DLN, providing further rationale to explore the immunologic implications of ENI.

To investigate these outstanding questions, we used the small-animal radiation research platform (SARRP) and developed a preclinical model of ENI that closely models the clinical practice of image-guided stereotactic radiotherapy (20). We evaluated two different radiotherapy strategies: (i) tumor-only stereotactic radiotherapy (Tumor RT) and (ii) ENI (T+LN RT) and dissected immunologic differences in the tumor microenvironment (TME). We quantified the function and magnitude of antigen-specific T-cell responses to ascertain whether one of the two radiotherapy strategies confer a relative advantage when combined with immune checkpoint blockade. As a number of clinical trials are exploring the combination of stereotactic radiotherapy with immunotherapy, it will be important to understand whether irradiation of the DLN modifies immunogenicity and potential synergy with immunotherapy.

Materials and Methods

Mice and cell lines

Animal experiments were performed using female 6- to 8-week-old mice housed in pathogen-free facilities accredited by the American Association for the Accreditation of Laboratory Animal Care (AAALAC) under protocols approved by the Animal Care and Use Committee of the Johns Hopkins University School of Medicine (Baltimore, MD). C57BL/6 wild-type mice were purchased from The Jackson Laboratory (Bar Harbor, ME). Adoptive T-cell transfer experiments were performed as previously described using congenically mismatched strains (21). Recipient CD45.1 (B6-Ly5.1) mice were purchased from Charles River Laboratories (Boston, MA). Donor OT-I/CD45.2/$Rag^{-/-}$ mice were bred in-house and have a transgenic T-cell receptor (TCR) that recognizes the H-$2K^b$–restricted class I epitope, ovalbumin (OVA) 257-264 (22).

MC38 colorectal carcinoma and B16/F10 melanoma cell lines were purchased from ATCC. MC38 and B16/F10 were cultured in complete (10% FBS, 1% antibiotic/antimycotic, 1% sodium pyruvate, and 1% MEM nonessential amino acids) RPMI and DMEM, respectively, in a 37°C, 5% CO_2 incubator. Some experiments used OVA antigen–expressing cell lines. MC38-OVA cells were a kind gift from Dr. Mark Smyth (QIMR Berghofer Medical Research Institute, Melbourne, Australia). B16-OVA cells were obtained from the laboratory of Dr. Hyam Levitsky (Johns Hopkins University, Baltimore, MD) and were cultured in RPMI complete media plus G418 (Sigma-Aldrich) for selection.

Intratumoral fluorescence tracking experiments, IHC, and immunofluorescence

For intratumoral fluorescence tracking experiments, tumor-bearing mice were injected with IRDye 800CW PEG contrast agent (LI-COR Biosciences) and serial *in vivo* near-IR imaging and image-guided surgery were performed as described previously (23). For IHC and immunofluorescence, tumors and DLNs were fixed with 4% paraformaldehyde for 48 hours at 4°C, snap frozen, and stored at −80°C before sectioning. Hematoxylin and eosin (H&E) staining was performed by the histology core facility (Johns Hopkins University, Baltimore, MD). Immunostaining for phospho-$H2AX^{ser139}$ (pH2AX) with DAPI nuclear counterstain was performed by an automated immunofluorescence (Ventana Medical Systems, Inc.) Molecular Cytology core facility (Memorial Sloan Kettering Cancer Center, New York, NY). Images were acquired on inverted fluorescence phase contrast microscope (Olympus IX-71).

In vivo stereotactic radiotherapy experiments

Flank tumors were established by subcutaneous (s.c.) or intradermal (i.d.) implantation of 1.5×10^6 MC38 or MC38-OVA or 5×10^5 B16 cells on day 0 into wild-type C57BL/6J (or B6-Ly5.1/CD45.1 recipient mice for adoptive transfer experiments). On day 11, tumor-bearing mice received 12Gy of stereotactic radiotherapy. α-PD-1 (murine IgG1, anti-PD-1 clone 4H2) and depleting α-CTLA4 (murine IgG2a, anti-CTLA4 clone 9D9) antibodies (200 μg) were a gift from Bristol-Myers Squibb under an

institutionally approved Material Transfer Agreement (MTA). Therapeutic antibodies were administered by intraperitoneal (i.p.) treatment on days 10, 12, and 14 (24). For time course experiments, mice were sacrificed on either day 11 (1 hour after radiotherapy), 13 (48 hours after radiotherapy) or 16 (120 hours after radiotherapy) as indicated. For studies focusing on therapeutic antibody administration, mice were sacrificed on day 21. Tumors and DLN were harvested and single-cell suspensions of tumor-infiltrating lymphocytes (TIL) and DLNs were prepared as described previously (15). Briefly, suspensions were prepared by mechanical dissociation, followed by density gradient centrifugation on an 80%/40% Percoll (GE Healthcare) gradient. Tumor mass (g) was measured as wet tumor weight on day of sacrifice. For rechallenge experiments, long-term survivors with complete responses to radiotherapy plus ICB were implanted with 1.5×10^6 MC38-OVA cells on the contralateral flank 6 months after initial tumor subcutaneous implant.

Stereotactic radiotherapy

Mice with well-established approximately 300 mm^3 tumors were irradiated with 12 Gy (3.0 Gy/minute) or sham nonirradiated, using the SARRP (Xstrahl) as described previously (20). Briefly, mice were anesthetized with isoflurane and underwent CT imaging on the SARRP for image-guided localization of the tumor (10-mm collimator) and DLN (3-mm collimator) with placement of isocenter prior to irradiation of the tumor alone or the tumor and DLN. Detailed radiation dosimetry and radiation planning information is provided in Supplementary Fig. S1.

Adoptive transfer experiments

Spleens and lymph nodes were harvested from OT-1/$Rag^{-/-}$ mice. Antigen-specific $CD8^+$ OT-1 T-cells were isolated by positive selection (CD8a MicroBeads, Miltenyi Biotec) and labeled with CFSE as per manufacturer's protocol (CellTrace CFSE kit, Thermo Fisher Scientific). CFSE-labeled $CD8^+$ OT-1 cells were resuspended in 200-μL PBS and transferred by retro-orbital injection (2×10^6 cells) on day 13 (48 hours after stereotactic radiotherapy) into congenic B6-Ly5.1/CD45.1 recipient tumor-bearing mice that had been implanted with 1.5×10^6 MC38-OVA cells on day 0. On day 16 (120 hours after radiotherapy, 72 hours after adoptive transfer), tumor and DLNs were harvested and immune cells were isolated as above and stimulated with 2 μmol/L H-$2K^b$–restricted class I epitope SIINFEKL $OVA_{257–264}$ (AnaSpec) in the presence of GolgiStop and GolgiPlug protein transport inhibitors (BD Biosciences) for intracellular cytokine staining and then analyzed by flow cytometry. As a positive control, mice were vaccinated with an attenuated *Listeria monocytogenes* vector engineered to express OVA (LM-OVA; Aduro Biotech; ref. 25). LM-OVA was diluted in PBS to 1×10^7 cfu per dose (0.1 LD_{50}), and administered by intraperitoneal injection (21).

Flow cytometry and tetramer staining

Single-cell suspensions prepared from DLNs and TILs were preincubated with mouse Fc Block-purified anti-mouse CD16/CD32 (BD Biosciences) for 30 minutes at 4°C. For tetramer staining, murine iTAg MHC Tetramer/PE H-2 K^b OVA (SIINFEKL) was purchased from MBL International and staining performed per manufacturer's instructions. For fluorochrome-conjugated antibodies, the following clones were used (purchased from BioLegend, except as noted): CD4 (GK1.5), CD8a (53–6.7), CD11b (M1/70; BD Biosciences), CD44 (IM7), CD45 (30-F11), CD45.2 (104), CD62L (MEL-14), FoxP3 (FJK-16s, eBioscience), IFNγ (XMG1.2), Ly-G6/Ly-6G Gr-1 (RB6-8C5), Live/Dead Fixable Aqua Dead Cell Stain Kit (Thermo Fisher Scientific), TNFα (MP6-XT22; BD Biosciences). Flow cytometry was performed using a BD LSR II instrument (BD Biosciences). Flow data were analyzed using FlowJo v10 software (Treestar, Inc.). Gating strategies are shown in Supplementary Fig. S2.

Luminex assay and ELISA

Tumors collected at specified posttreatment time points were mechanically dissociated, lysed, and incubated on ice for 30 minutes with intermittent vortexing in CellLytic MT Cell Lysis Reagent (Sigma-Aldrich) containing Halt Protease and Phosphatase Inhibitor (Thermo Fisher Scientific) in a 1:100 ratio. Tumor lysates were assayed for raw protein concentration using a Coomassie assay (Bio-Rad). Intratumoral chemokines and cytokines were quantified using the Bio-Plex Pro mouse chemokine panel assay (Bio-Rad) and the multiplex MCYTOMAG-70K multiplex assay (EMD Millipore). Luminex assays were conducted as per manufacturer's instructions. For ELISA experiments, TILs were stimulated overnight with OVA peptide and supernatants were collected and target cytokines were measuring using eBioscience mouse IFNγ, TNFα and IL-2 ELISA Ready-Set-Go! Kits (Thermo Fisher Scientific). For IL-7 experiments, serum and supernatant derived from inguinal nodal lysate (ipsilateral to tumor) was collected and measured per manufacturer's instructions using Mouse IL-7 ELISA kit (Thermo Fisher Scientific).

Venous blood collection for complete blood counts (whole-blood hematology)

Serial complete blood counts with differential cell subset analysis were performed by collecting 100-μL whole blood via tail vein puncture into K_2EDTA-coated BD Vacutainer microcollection tubes (Becton, Dickinson and Company). Tubes were inverted/mixed 8–10 times, directly transported at room temperature to the core facility (Institute of Comparative Medicine at Columbia University) and analyzed using the Genesis Veterinary Hematology System (Oxford Science Inc.).

Statistical analysis

Statistical analyses were performed using GraphPad Prism 6 (GraphPad Software). Significance was calculated as described in figure legends. Results were considered statistically significant at $P \leq 0.05$ (*).

Results

Image-guided stereotactic elective nodal irradiation (ENI) accurately targets tumor-associated DLN

We first developed a model to quantify immunologic differences between two radiotherapy strategies: (i) stereotactic radiotherapy delivered to the tumor-only (Tumor RT) and (ii) stereotactic radiotherapy delivered to the tumor and the tumor-associated DLN (T+LN RT). To identify the tumor-associated DLNs, we performed intratumoral injection of a fluorescent dye (IRDye 800CW PEG contrast agent) in C57BL/6J mice implanted with B16 melanoma or MC38 colorectal carcinoma flank tumors. Serial fluorescent imaging was performed after intratumoral administration; accumulation of fluorescence within the ipsilateral inguinal DLNs was noted after 1 hour (Fig. 1A and B).

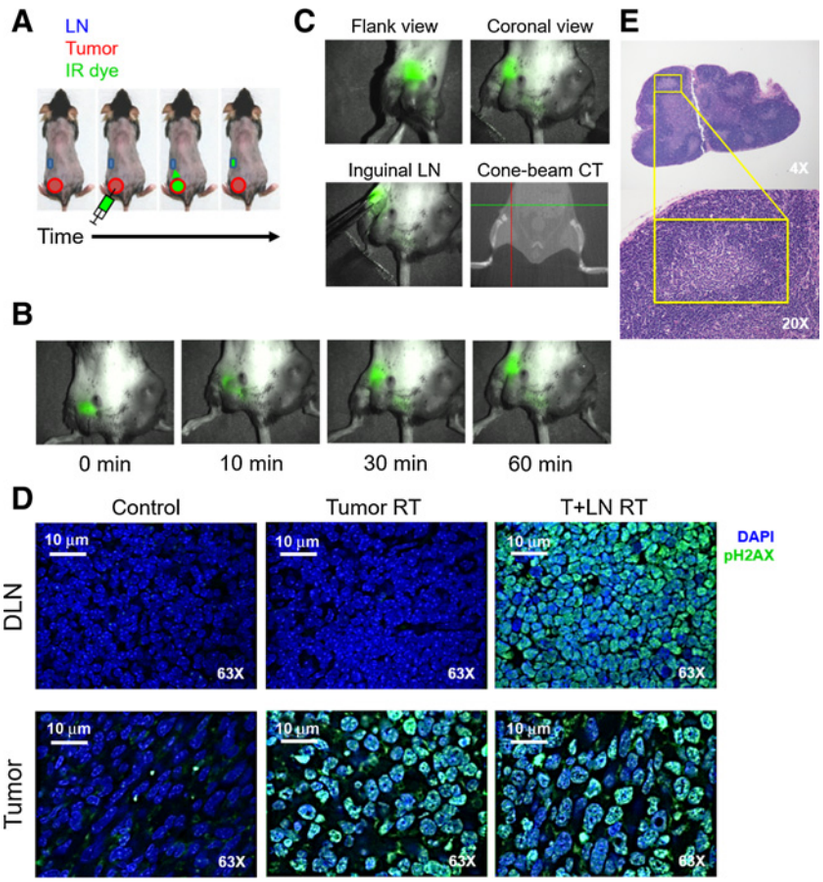

Figure 1.

A preclinical model of image-guided ENI accurately targets the tumor-associated DLN. **A,** Schematic of intratumoral dye injection, transit, and accumulation in ipsilateral tumor-associated inguinal lymph node (DLN). **B,** Lymphatic tracking of fluorescent dye (IRDye 800CW PEG contrast agent) following intratumoral administration on day 11 in tumor-bearing C57BL/6J mice inoculated by s.c. or i.d. flank injection with 5×10^5 B16F10 or 1.5×10^6 MC38 cells ($n = 2$–3 mice per experiment, repeated twice). **C,** Representative images of fluorescent dye–guided surgery isolating ipsilateral inguinal DLN and coronal view cone-beam CT image with crosshairs overlying inguinal fat pad. **D,** Immunofluorescence detection (63× magnification) of phospho-H2AX^{ser139} (green) and DAPI (blue) nuclear staining in nonirradiated (control) and irradiated mice (Tumor RT or T+LN RT). Tumor and DLN tissue harvested 1 hour after 12 Gy × 1. **E,** Representative H&E stain (4–20× magnification) of inguinal DLN harvested from untreated B16F10 tumor-bearing mouse ($n = 3$) on postinoculation day 14 depicting absence of tumor cells.

Fluorescence-guided surgery confirmed that the majority of the dye had trafficked from the tumor into the ipsilateral inguinal node, supporting that particular node as the predominant tumor-associated DLN in these models (Fig. 1C). In subsequent experiments, cone-beam CT imaging using the SARRP reliably visualized the inguinal fat pad, allowing for delivery of image-guided stereotactic radiotherapy to the tumor-associated DLNs as a model for ENI (Fig. 1C; Supplementary Fig. S1).

To validate the ability of SARRP-based radiotherapy to accurately target or spare the DLN, we assessed induction of phospho-H2AX (pH2AX) nuclear foci as a surrogate for radiation-induced DNA double-stranded breaks (26). Tumor and DLNs were harvested from irradiated mice 1 hour after 12 Gy ×1 (or sham radiotherapy), delivered stereotactically. Tumor RT demonstrated clear induction of pH2AX foci in the tumor and an absence of pH2AX foci in the DLN while T+LN RT demonstrated induction of pH2AX foci in both the tumor and DLN, verifying targeted delivery of stereotactic radiotherapy (Fig. 1D). To assess whether the DLNs were involved with tumor, a board-certified surgical pathologist (R.A. Anders) confirmed the absence of metastatic disease in the tumor-associated DLN of untreated mice on day 14 (Fig. 1E); this was critical given that ENI is a strategy used in clinically localized tumors that do not have evidence of locoregional metastases (16–18). In subsequent studies, stereotactic radiotherapy was delivered on day 11 (tumor volume ~200–300 mm^3), thus animals were unlikely to harbor gross nodal metastases at the time of treatment.

ENI decreases tumor-infiltrating immune cell density relative to tumor-only stereotactic radiotherapy

We next performed a series of experiments to qualitatively and quantitatively test for differences in tumor-infiltrating immune cell phenotype between Tumor RT and T+LN RT. Relative to untreated mice (control), Tumor RT significantly ($P < 0.001$) enhanced the intratumoral density of effector (CD44$^+$ CD62L$^-$) CD8$^+$ T cells (CD8$^+$ effector, Fig. 2A, left). Tumor RT also significantly increased ($P < 0.001$) the absolute number (per gram tumor) of intratumoral FoxP3$^+$ CD4$^+$ T cells (Tregs) and CD11b$^+$ Gr-1^{hi} myeloid cells (Fig. 2B and C, left). In sum, the addition of radiotherapy to the DLN (T+LN RT) was associated with a statistically significant decrease ($P < 0.001$) in the intratumoral density of all three immune cell subsets (CD8 effectors, Tregs, and CD11b$^+$ Gr-1^{hi} myeloid cells) as compared with Tumor RT (Fig. 2A–C, left).

Normalized to the control group, there were significant ($P < 0.001$) 12.5-fold and 4.0-fold increases in intratumoral density of CD8 effectors and Tregs in the Tumor RT group, respectively (Fig. 2D). T+LN RT was not associated with a significant modulation of either tumor-infiltrating subset with a 2.1-fold increase in CD8$^+$ effectors and no change in Tregs. Nevertheless, both Tumor RT and T+LN RT increased the CD8 effector-to-Treg ratio, relative to nonirradiated controls (Fig. 2D). When comparing radiotherapy strategies, the CD8 effector-to-Treg ratio was significantly greater with Tumor RT ($P = 0.001$, Tumor RT 8.8 vs. T+LN RT 6.3). Taken together, these findings show that irradiation of the DLN has a

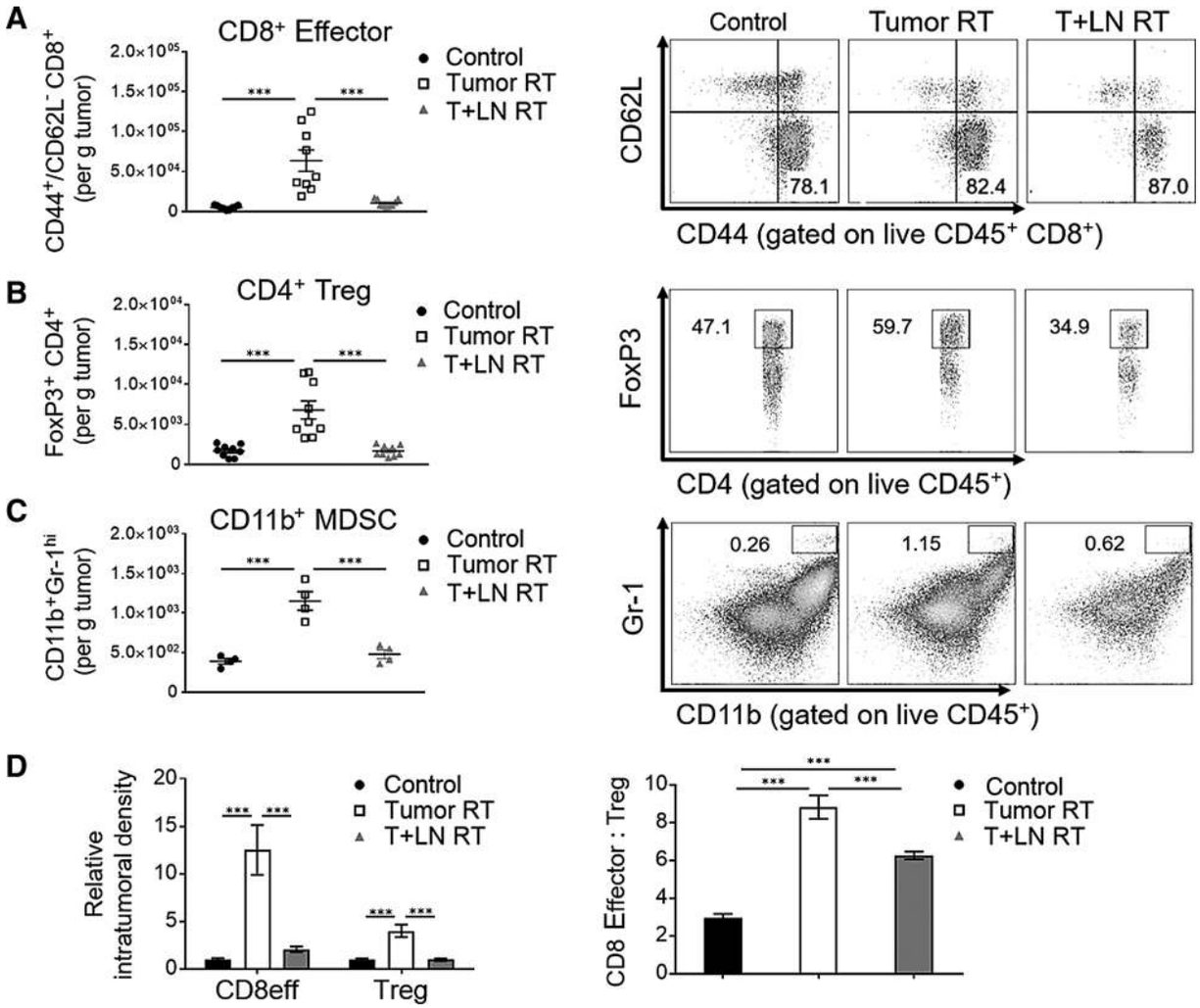

Figure 2.

ENI decreases tumor-infiltrating immune cell density relative to tumor-only stereotactic radiotherapy. Flank tumor–bearing mice untreated or irradiated (12 Gy ×1) to tumor-only (Tumor RT) or tumor and DLN (T+LN RT) on day 11 following s.c. injection of 1.5×10^6 MC38 tumor cells ($n = 4$–9 mice per group, repeated 2–3 times). Tumors were harvested for analysis on day 16, 120 hours after treatment. **A–C,** Representative quantitative scatterplot and flow cytometry demonstrating absolute number of tumor-infiltrating immune cells and percentage ($CD8^+$ effector, $CD44^+$ $CD62L^-$ $CD8^+$; Treg, $CD4^+$ $FoxP3^+$; myeloid-derived suppressor cells, CD11b+ $Gr\text{-}1^{hi}$) per gram of tumor in MC38 tumor model. **D,** Fold change of CD8 effector and Treg subsets by treatment group, normalized to control group. Quantitative bar graph of CD8 effector-to-Treg ratio by treatment group. Error bars, SEM. ***, $P < 0.001$, treatment group comparisons by one-way ANOVA and *post hoc* Tukey multiple comparison test.

significant impact on immune infiltration of the TME and that multiple immunologic differences exist between Tumor RT as compared with T+LN RT.

Tumor RT and T+LN RT have distinct radiation-induced intratumoral chemokine expression and $CD8^+$ T-cell trafficking patterns

We next sought to elucidate the mechanisms underlying the differences in intratumoral immune infiltration between radiotherapy strategies. Time course experiments demonstrated a significant ($P < 0.001$) increase in the absolute number of viable $CD45^+$ cells within the tumor-associated DLN 48 hours after Tumor RT (Supplementary Fig. S3); this was not observed in the control or T+LN RT groups. Further dissection of the $CD45^+$ population demonstrated that this was predominantly driven by an increase in the total number of $CD8^+$ T cells at the 48-hour time point, that is, we observed a 2.5-fold increase relative to the untreated control and 2.2-fold increase relative to the T+LN radiotherapy group (Fig. 3A). At these postradiotherapy time points, Luminex multiplex immunoassay of tumor lysate demonstrated a distinct pattern of upregulation of chemokines associated with T-cell chemoattraction; this was observed predominantly in the Tumor RT group (Fig. 3B). Specifically, 48 hours after Tumor RT, there was a significant upregulation of CXCR3 and CCR5-associated chemokines (i.e. CXCL10, CCL3, CCL5), which have been shown to be important for recruitment of antigen-specific $CD8^+$ effector T cells into the tumor microenvironment (9–10, 27–29). This

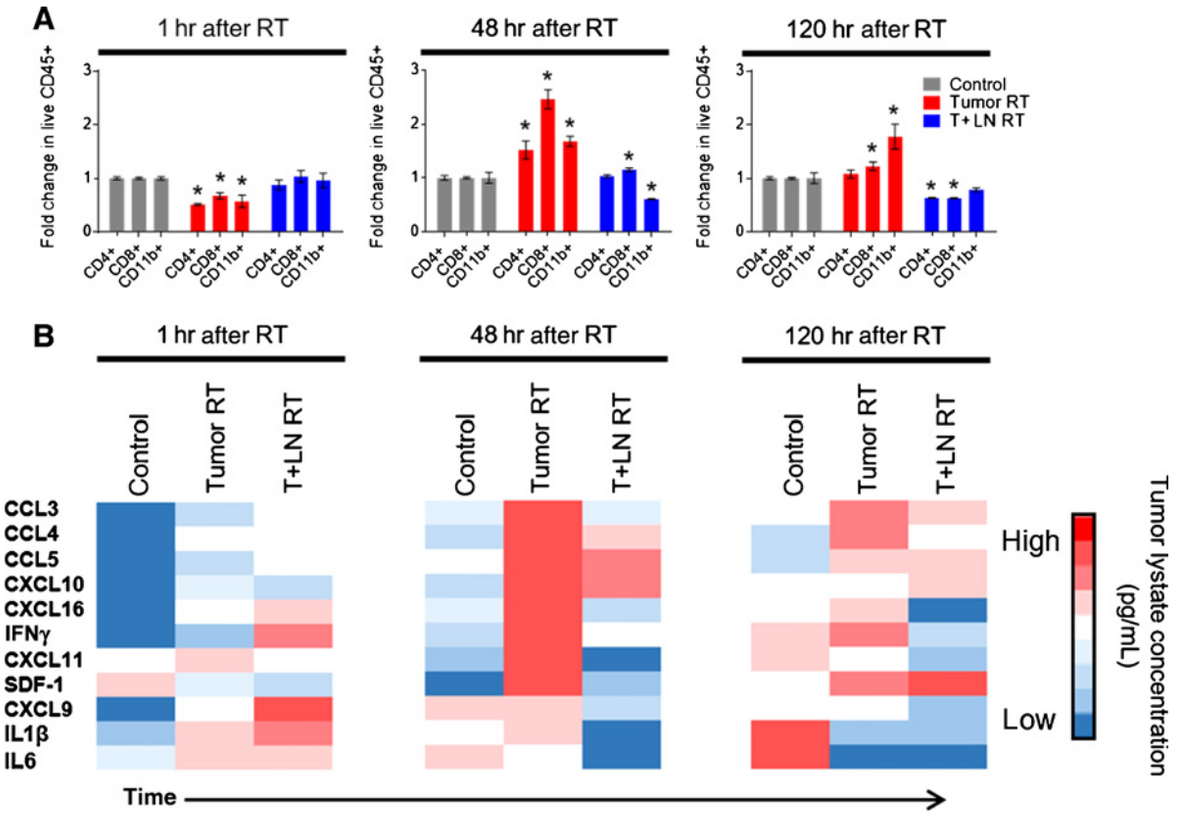

Figure 3.

Tumor RT and T+LN RT have distinct radiation-induced intratumoral chemokine expression and CD8$^+$ T-cell trafficking patterns. **A,** Tumor-associated DLN of MC38 tumor-bearing mice harvested at 1 hour, 48 hours, and 120 hours after treatment with Tumor RT or T+LN RT on day 11. Quantitative bar graphs representing fold change of absolute number of CD4$^+$, CD8$^+$, and CD11b$^+$ immune cell subsets in tumor-associated DLN over time, normalized with control ($n = 12$ mice per group with 4 mice per time point, repeated twice). **B,** Tumor lysate collected at same postradiotherapy timepoints as Fig. 3A and analyzed by Luminex multiplex immunoassay. Colorimetric heatmap conditional formatting with blue to red indicating low to high chemokine/cytokine concentration (pg/mL), respectively. Error bars represent SEM; *, $P < 0.05$, CD45$^+$ immune cell and chemokine expression time course experiments analyzed by two-way ANOVA and *post hoc* Tukey multiple comparison test.

upregulation of intratumoral chemokines was attenuated in T+LN RT–treated mice. Untreated (control) tumors demonstrated increased expression of IL1β and IL6 over time, which has been associated with poor prognosis, tumor progression, and immunosuppression (30–32). Complete quantitative data are provided in Supplementary Fig. S3. Collectively, these data suggest that ENI attenuates radiotherapy-mediated chemokine expression in the TME; this decreased chemokine expression may explain reduced CD8 effector infiltration in the T+LN group.

Radiation-mediated tumor infiltration with functional antigen-specific CD8$^+$ T cells is restrained by ENI

Given that radiation enhances cross-priming of antigen-specific CD8$^+$ effector T cells primarily within the tumor-associated DLNs (14–15), we queried whether T+LN RT (ENI) alters the effector function of antigen-specific T cells in the tumor microenvironment. For these experiments, we used MC38-OVA and B16-OVA tumors, with the notion that in this system, OVA models a mutation-associated neoantigen (MANA) to which high-affinity T cells may exist (33). To quantify antigen-specific T-cell responses, we performed adoptive transfer experiments in which naïve CFSE-labeled OVA-specific CD8$^+$ T cells (OT-1) were transferred into host mice bearing OVA-expressing tumors 48 hours after stereotactic radiotherapy. For a positive control, we transferred cells to a nonirradiated, nontumor-bearing mice and vaccinated recipients with LM-OVA, this resulted in >90% T-cell division with >50% of divided cells positive for IFNγ (Supplementary Fig. S3C).

Consistent with the chemokine data in Fig. 3, we found that Tumor RT versus T+LN RT resulted in significant differences in immunologic parameters in the TME. The absolute number (per gram tumor) of effector cytokine-producing, dividing OT-1 cells was significantly greater ($P < 0.001$) in the Tumor RT group (Fig. 4A, left). Endogenous (CD45.2-negative) CD8 T cells (Fig. 4A, center) showed a similar pattern. These findings were supported by ELISA data (Fig. 4A, right) showing that the concentration of IFNγ and TNFα in the supernatant collected from OVA-stimulated TILs was significantly increased in the Tumor RT group relative to both control ($P < 0.001$) and T+LN RT ($P < 0.001$). Corroborating these results with endogenous antigen-specific T cells, H-2kb OVA (SIINFEKL) tetramer staining showed

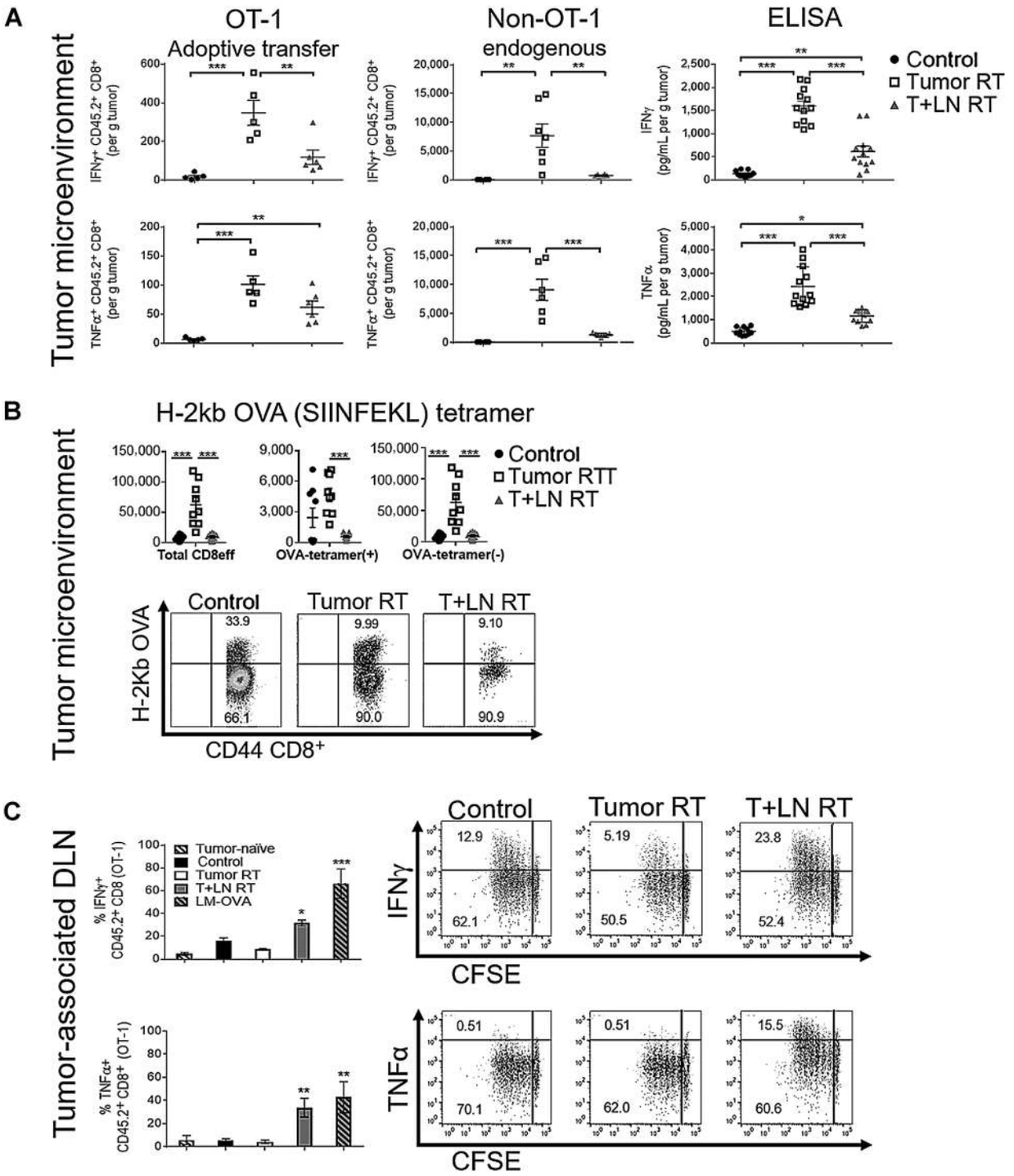

Figure 4.

Radiation-mediated tumor infiltration with functional antigen-specific CD8$^+$ T cells is restrained by ENI. A total of 2×10^6 CFSE-labeled, OVA-specific CD8$^+$ T cells from donor Rag$^{-/-}$/OT-1 TCR transgenic CD45.2 mice were adoptively transferred (AT) into MC38-OVA tumor-bearing congenically mismatched CD45.1 C57BL/6J mice on day 13. CD45.1 mice were treated on day 11 (48 hours before AT) with control, Tumor RT, and T+LN RT, with DLN and tumor harvested on day 16, 120 hours after radiotherapy (AT, $n = 5$–9 mice per group, repeated 3 times). **A,** Quantitative scatter plots of effector cytokine production by tumor-infiltrating OT-1, endogenous CD8$^+$ T cells via intracellular cytokine staining and ELISA (top rows, L to R, respectively). **B,** Absolute number of tumor-infiltrating CD8$^+$ CD44$^+$ T cells per gram tumor by H-2kb OVA (SIINFEKL) tetramer staining and representative flow cytometry plots (ELISA and tetramer staining, $n = 5$ per group, repeated twice). **C,** Bar graphs and representative flow plots of effector cytokine production (IFNγ, TNFα) by AT CD45.2$^+$ CD8$^+$ T cells in tumor-associated DLNs. Error bars represent SEM; ***, $P < 0.001$; **, $P < 0.01$; *, $P < 0.05$, treatment group comparisons by one-way ANOVA and *post hoc* Tukey multiple comparison test.

that Tumor RT significantly enhanced the absolute number of tumor-infiltrating tetramer-positive $CD8^+$ effectors as compared with T+LN RT ($P < 0.001$; Fig. 4B, middle). As expected, the tumor-infiltrating $CD8^+$ effector population was largely comprised of tetramer-negative cells (Fig. 4B, right). Furthermore, endogenous effector (non-OT-1) $IFN\gamma^+/TNF\alpha^+$ $CD8^+$ T cells were significantly enriched in the Tumor RT group, supporting that non-OVA–specific intratumoral T cells were also potentially functional (Fig. 4A, middle). Taken together, these data show that radiotherapy to the tumor alone (as compared with T+LN RT) was associated with increased intratumoral infiltration of both antigen-specific as well as additional effector T cells.

Turning to the DLNs, we found that there were no significant differences in OT-1 division in the DLN between Tumor RT and T+LN RT (Supplementary Fig. S3C). However, the proportion of effector cytokine-producing divided OT-1 cells was significantly decreased ($IFN\gamma^+$, $P < 0.05$; $TNF\alpha^+$, $P < 0.001$) in the DLNs of mice treated with Tumor RT alone as compared with T+LN RT (Fig. 4C). Thus, the findings in the DLN suggested that T+LN RT may not limit the initial priming of antigen-specific T cells. However, it is notable that this radiotherapy strategy (ENI) was associated with a significant reduction in the intratumoral accumulation of antigen-specific functional CD8 effectors. This contrasts the finding of increased $CD8^+$ T-cell infiltration into the TME associated with Tumor RT alone (Fig. 4A and B) and further supports the concept that radiotherapy target/site alters T-cell migration and effector function.

ENI attenuates combinatorial efficacy between radiation and immunotherapy

As significant immunologic differences were observed between Tumor RT and T+LN RT, we next explored whether these differences would be reflected in a therapeutic model of stereotactic radiotherapy, either alone or in combination with immune checkpoint blockade (Fig. 5A). For these studies, we used a blocking PD-1 antibody (clone 4H2) and an IgG2a isotype CTLA4 antibody; the latter reagent partially depletes Tregs in the TME reflecting the IgG1 isotype of the FDA-approved anti-CTLA4 agent (ipilimumab; ref. 24). While Tumor RT and T+LN RT each increased median survival compared with untreated controls (isotype), neither approach resulted in complete tumor regression or long-term survival. Tumor RT prolonged median survival relative to T+LN RT ($P < 0.001$; 41 vs. 25 days); however, all tumors eventually recurred (Fig. 5B–D). When combined with

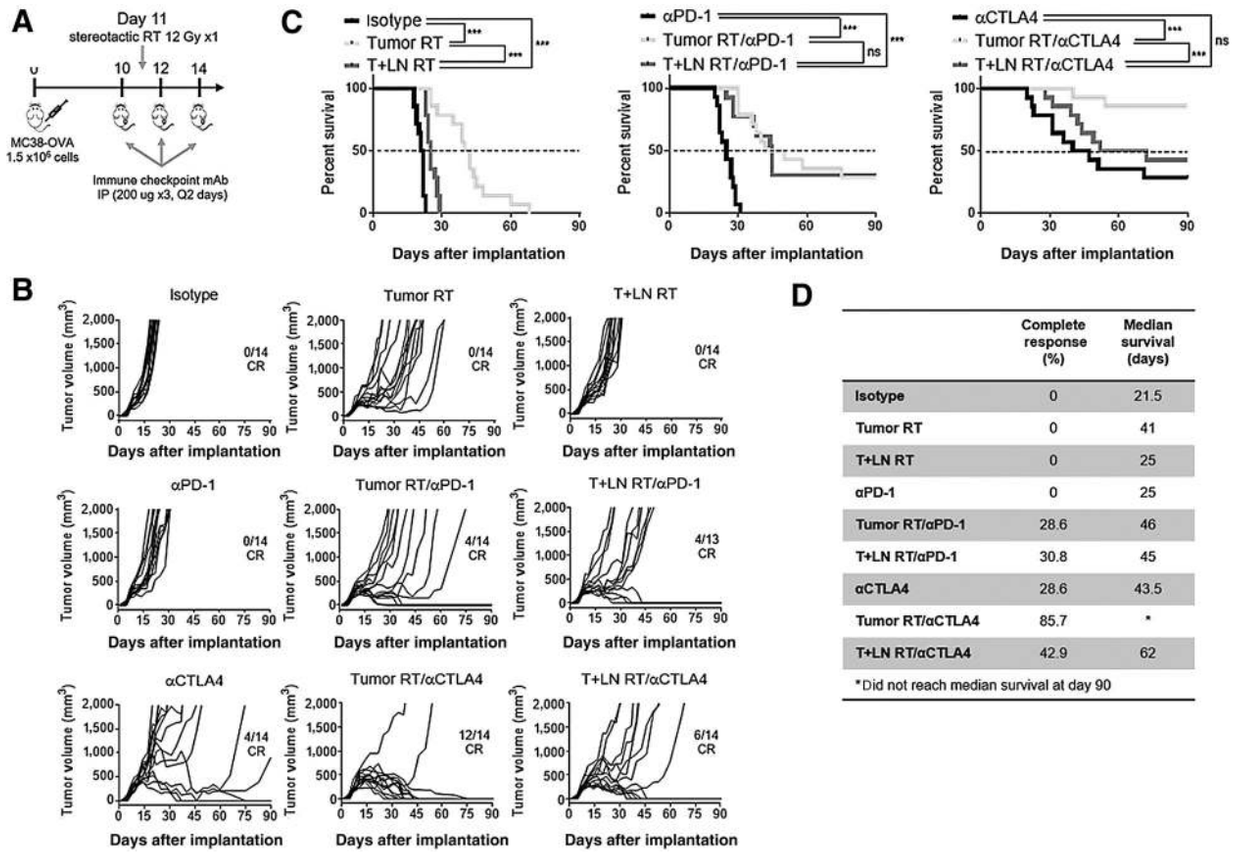

D

	Complete response (%)	Median survival (days)
Isotype	0	21.5
Tumor RT	0	41
T+LN RT	0	25
αPD-1	0	25
Tumor RT/αPD-1	28.6	46
T+LN RT/αPD-1	30.8	45
αCTLA4	28.6	43.5
Tumor RT/αCTLA4	85.7	*
T+LN RT/αCTLA4	42.9	62

*Did not reach median survival at day 90

Figure 5.

ENI attenuates combinatorial efficacy between radiation and immunotherapy. **A,** Treatment schema: Tumor RT or T+LN RT (12 Gy ×1) administered on day 11 and three doses (i.p. 200 μg) of therapeutic antibody (isotype, αPD-1, αCTLA4) on days 10, 11, and 12 in MC38-OVA tumor-bearing mice ($n = 6$–7 per group, repeated twice). **B,** Spider plots of tumor outgrowth (mm^3) by treatment group, annotated with number of complete responses (CR) over total mice treated. **C,** Percent survival by treatment group at day 90 after s.c. flank injection of MC38-OVA tumor cells. **D,** Summary table of % CR and median survival by treatment corresponding to **B** and **C**. Kaplan–Meier analysis with log-rank (Mantel–Cox) test for survival differences between treatment groups (***, $P < 0.001$).

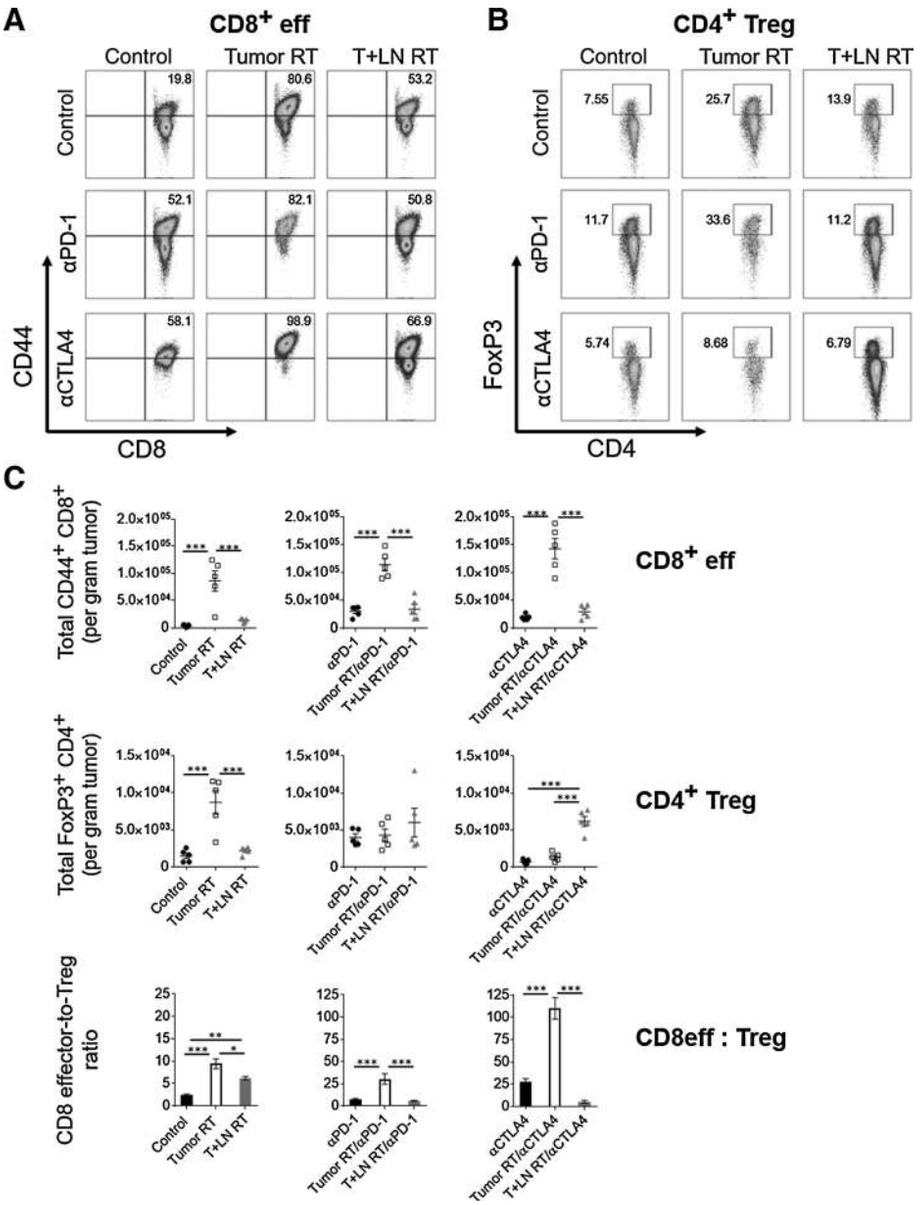

Figure 6.
Favorable modulation of intratumoral CD8 effector-to-Treg ratio is associated with long-term survival. MC38-OVA tumor-bearing mice treated per schema in Fig. 5A; tumors harvested day 21 after subcutaneous flank injection ($n = 5$ per group). **A** and **B,** Representative flow cytometry (left, CD8 effectors; right, Tregs) and quantitative scatterplots (**C**, top and middle), demonstrating percentage and absolute number of tumor-infiltrating immune cells per gram of tumor by treatment group, respectively. **C,** Quantitative bar graph (bottom) of CD8 effector-to-Treg ratio by treatment group. Error bars represent SEM (***, $P < 0.001$; **, $P < 0.01$; *, $P < 0.05$), treatment group comparisons by one-way ANOVA and *post hoc* Tukey multiple comparison test.

PD-1 blockade, both radiotherapy strategies conferred a survival advantage relative to αPD-1 monotherapy, with a complete response rate of 29% and 31% in Tumor RT/αPD-1 and T+LN RT/αPD-1, respectively. However, there were no differences in median survival or response rate between combination therapies with radiotherapy + αPD-1. In the context of concurrent αCTLA4, ENI adversely impacted survival (24). Tumor RT/αCTLA4 yielded a complete response rate of 86% and median survival had not been reached by day 90. In the T+LN RT/αCTLA4 group, irradiation of the tumor-associated DLNs significantly reduced median survival (62 days) and complete response rate (43%) relative to Tumor RT/αCTLA4 ($P < 0.001$), similar to the response rate observed for both radiotherapy + αPD-1 combinations (Fig. 5D). Notably, in this established MC38-OVA model (day 11), αPD-1 monotherapy was largely ineffective and yielded no complete responses (34). Conversely, αCTLA4 monotherapy induced complete tumor regression in 29% of mice. Despite differences in efficacy between αPD-1 and αCTLA4, a negative association of ENI upon survival was evident when comparing T+LN radiotherapy versus Tumor RT as well as T+LN RT/αCTLA4 versus Tumor RT/αCTLA4.

Favorable modulation of intratumoral CD8 effector-to-Treg ratio is associated with long-term survival

To quantify immunologic parameters associated with response to combination therapy with stereotactic radiotherapy and ICB, we performed immunophenotyping to evaluate differences in intratumoral immune modulation between treatment groups. It should be noted that these studies focused on well-established tumors (day 11, ~300 mm^3); as above, PD-1 blockade is generally

ineffective as a monotherapy for late-stage MC38 tumors (34). Broadly, our findings suggested that the absolute number (per gram tumor) of intratumoral CD8 effectors and as well as a favorable CD8 effector-to-Treg ratio correlate with a survival benefit. The Tumor RT/αCTLA4 group, which yielded the greatest number of complete responses and longest median survival, was found to have a significantly elevated CD8 effector-to-Treg ratio (110.1); this was substantially greater than all other treatment groups (Fig. 6C, bottom). Similar to our prior findings (see Fig. 2), Tumor RT was associated with a significant increase in the intratumoral density of CD8 effectors and Tregs relative to control and to T+LN RT (Fig. 6C, left top/middle; all $P < 0.001$). In the context of ICB with either αPD-1 or αCLTA4, Tumor RT significantly enhanced CD8 effector infiltration relative to either ICB monotherapy (all $P < 0.001$) and also enhanced CD8 effector infiltration relative to T+LN RT when combined with αPD-1 or αCLTA4 (all $P < 0.001$), respectively (Fig. 6C, top). PD-1 blockade appeared to have a modest impact on the Treg subsets in this model (Fig. 6C, middle/center). However, αCTLA4 as a monotherapy or in combination with Tumor RT decreased intratumoral Tregs (24, 35–36). In contrast, when T+LN RT was combined with αCTLA4, there was a significant increase in intratumoral Tregs, relative to both Tumor RT and control (both $P < 0.001$, Fig. 6C, right middle). Taken together, the ability of αCTLA4 IgG2a to enhance CD8 effectors and reduce Tregs promoted the proimmunogenic effects of Tumor RT and limited its immunosuppressive effects, thereby favorably increasing the CD8 effector-to-Treg ratio (Fig. 6C, bottom).

Improved resistance to rechallenge in animals treated with radiotherapy + αCTLA4

We next set out to assess the longer-term outcome of radiotherapy technique in the presence or absence of ICB. On day 21 posttumor inoculation (day 10 postradiotherapy), H-2kb OVA tetramer analysis of tumors harvested after treatment with Tumor RT/αCTLA4 demonstrated the most robust infiltration of OVA-specific $CD8^+$ effectors. Indeed, the intratumoral density of antigen-specific $CD8^+$ effectors with this pairing was 3-fold greater than any other treatment group (Fig. 7A). With regards to effector cytokine production in response to OVA peptide stimulation, intratumoral IFNγ expression most strongly correlated with the density of antigen-specific immune cells as well as survival (Fig. 7B; ref. 37).

Finally, to functionally ascertain whether the development of a protective memory response was influenced by treatment type, we rechallenged surviving mice a full 6 months (180 days) after initial tumor implantation. For these studies, the only animals that achieved long-lasting complete responses were those treated with combined stereotactic radiotherapy and ICB. As mentioned, >85% of mice treated with Tumor RT/αCTLA4 achieved complete responses/long-term survival while long-term survival with other combination RT/immunotherapy groups ranged 28%–43% (Fig. 5D); therefore, the initial combination radiotherapy/immunotherapy strategy influenced survival and thus the ability to be rechallenged. When stratifying the subset of long-term survivors by ICB type, mice previously treated with a αCTLA4-based combination regimen (Tumor RT/αCTLA4 and T+LN RT/αCTLA4) were more resistant to rechallenge (Fig. 7C). Specifically, 100% of the prior αCTLA4-treated group survived rechallenge, while by comparison 50% of prior αPD1-treated animals survived rechallenge (Fig. 7C). Among the αPD1-treated mice that were unable to clear tumor, there was a significant tumor growth delay ($P = 0.003$, median survival 51 vs. 22 days) relative to tumor implantation in naïve host animals (Fig. 7C). When stratifying by initial radiotherapy strategy (Tumor RT vs. T+LN RT), there was no appreciable impact on subsequent tumor rejection in the context of rechallenge (Fig. 7C).

Discussion

The optimal delivery of stereotactic radiotherapy to promote immunogenicity remains an open area of investigation. Specifically, it is currently unknown whether irradiating the tumor-associated DLN modulates adaptive immunity and therefore the potential of radiotherapy to effectively synergize with immunotherapy. Here, we developed a preclinical model of elective nodal irradiation (ENI), acknowledging that we verified the absence of nodal micrometastases by histopathology. We used this model to evaluate the immunologic implications of stereotactic radiotherapy strategies that either target or spare the tumor-associated DLNs. One important feature of these studies is our use of the SARRP, which allowed for these preclinical *in vivo* radiotherapy studies to model the delivery of image-guided radiotherapy in clinical practice. To further enhance the clinical relevance and rigor of our model, fluorescence-guided surgery performed after intratumoral injection of a fluorescent dye identified the inguinal lymph node as the predominant tumor-associated DLN (Fig. 1A). This is akin to lymphatic mapping which is commonplace in breast cancer or melanoma as intratumoral radiotracer and/or dye are used to identify the sentinel DLN.

We found that Tumor RT and ENI (T+LN RT) yielded distinct intratumoral chemokine expression profiles which were associated with significant differences in immune infiltration of the TME. Consistent with the existing literature, Tumor RT was associated with significant upregulation of CXCL10, CXCL16, and other CCR5-related chemokines (Fig. 3B, Supplementary Fig. S3B). Radiotherapy-mediated type I/II IFN signaling appears to be important for increased intratumoral CXCL10 levels (IFNγ-induced protein 10, IP-10) which correlates with intratumoral accumulation of $CD8^+$ T cells (27, 29). It was recently demonstrated that the CXCL10/CXCR3 chemokine–chemokine receptor axis is required for intratumoral CD8 effector T-cell homing from the DLNs and periphery (28). Matsumura and colleagues demonstrated the radiotherapy-induced CXCL16 secretion from irradiated breast cancer cells specifically recruit $CD8^+$ effector T cells expressing the cognate CXCR6 chemokine receptor (10). In addition, enhanced intratumoral expression of CXCL10 and CCL5 was observed following tumor irradiation in a Panc02-SIY pancreatic tumor model (38). Taken together, our findings suggest that Tumor RT induces an intratumoral T-cell chemoattractant chemokine signature that promotes robust infiltration of functional $CD8^+$ effector T cells.

Our most striking finding was that radiotherapy-mediated chemokine expression was attenuated by ENI (T+LN RT), leading to impaired trafficking of $CD8^+$ T cells into the TME and, ultimately, decreased survival in our therapeutic model (Figs. 1A and 4D). Given those findings, we also considered a potential contribution of direct lymphotoxic effects upon the irradiated DLNs. We noted a modest decline in live $CD45^+$ cells within the irradiated DLN (Fig. 3A; Supplementary Fig. S3A). Systemically, we noted a modest decline in circulating lymphocytes among

irradiated mice but did not observe significant differences in peripheral lymphocyte counts between Tumor RT and T+LN RT nor indication of severe treatment-related lymphopenia (Supplementary Fig. S4A). However, a contributory effect of lymphodepletion cannot be entirely excluded in this model. Arguing against this possibility, T+LN RT was associated with the highest

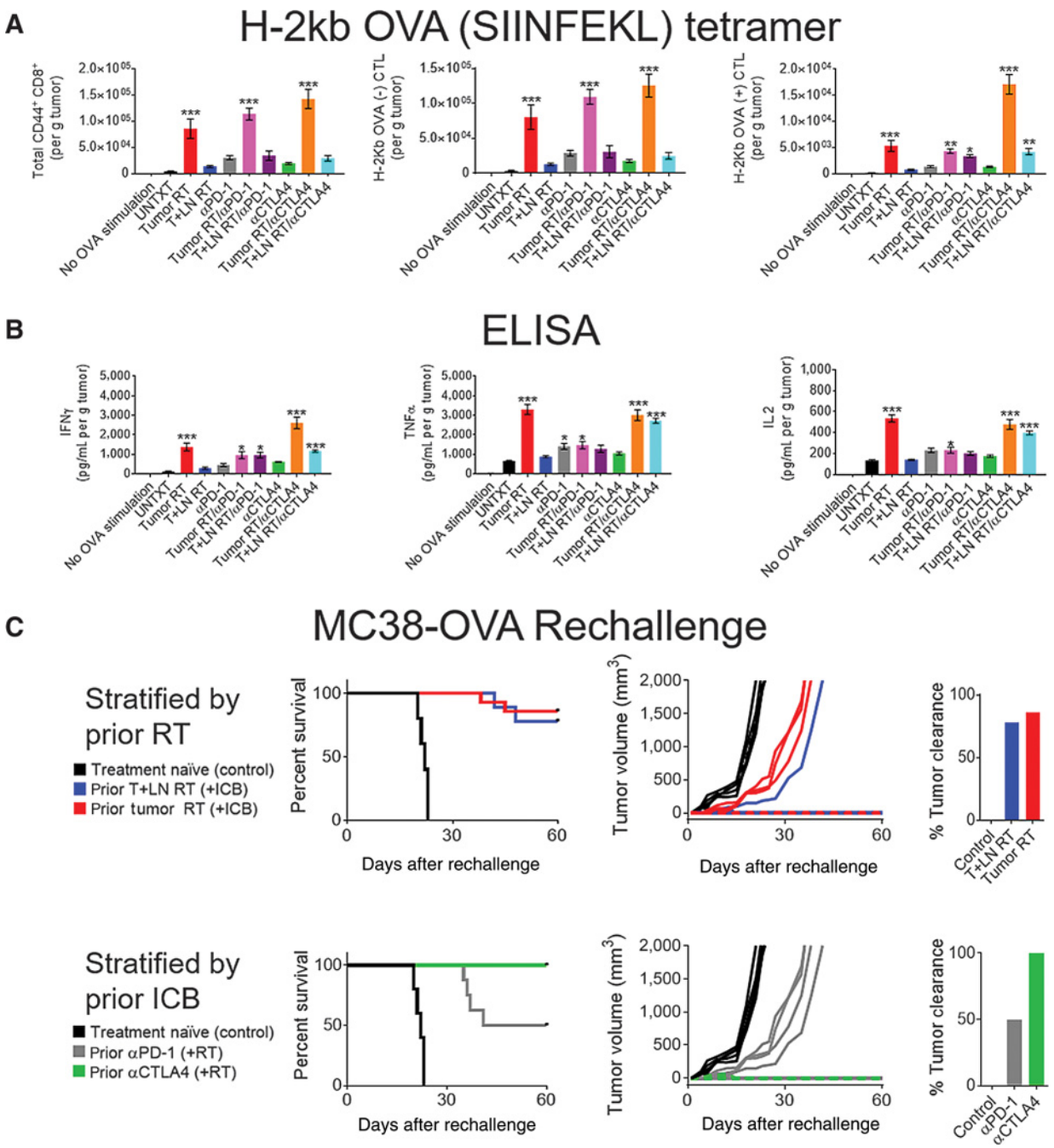

Figure 7.

Improved resistance to rechallenge in animals treated with radiotherapy + αCTLA4. MC38-OVA tumor-bearing mice treated per schema in Fig. 5A. Tumors harvested on day 21 after subcutaneous flank injection ($n = 5$ per group). **A,** Absolute number of antigen-specific tumor-infiltrating $CD8^+$ $CD44^+$ T cells per gram tumor by H-2kb OVA (SIINFEKL) tetramer staining. **B,** Measurement of cytokine concentration (pg/mL per gram tumor) by ELISA in TIL-derived supernatant. **C,** Long-term survivors with complete responses previously treated with combined radiotherapy and ICB were rechallenged on the contralateral flank with 1.5×10^6 MC38-OVA tumor cells 180 days after initial tumor subacutaneous implant; spider plots, % survival and % tumor clearance stratified by prior radiotherapy strategy or prior ICB received (treatment-naïve, $n = 5$; Tumor RT, $n = 11$ vs. T+LN RT, $n = 9$; αPD-1, $n = 8$ vs. αCTLA4, $n = 15$). Error bars represent SEM (***, $P < 0.001$; **, $P < 0.01$; *, $P < 0.05$), treatment group comparisons by one-way ANOVA and *post hoc* Tukey multiple comparison test.

proportion of dividing antigen-specific cells and the greatest number of IFNγ$^+$ and TNFα$^+$ antigen-specific CD8$^+$ T cells within the tumor-associated DLNs (Fig. 4C). These data suggest that there was a pool of functional antigen-specific CD8$^+$ T cells present within the DLN that ultimately did not traffic into the TME when the DLN was irradiated (Figs. 3A and 4A and B). In support of this finding, Mikucki and colleagues demonstrated that adoptively transferred CXCR3$^{-/-}$-deficient OT-1 cells have limited intratumoral localization capacity relative to wild-type OT-1 counterparts despite having equivalent cytotoxic activity and effector cytokine (IFNγ and granzyme B) production (28). Taken together, our findings suggest that the irradiation of the DLNs disrupts the chemokine-driven orchestration of effector T-cell recruitment into the TME. These novel observations regarding ENI improve our understanding of radiotherapy-mediated adaptive antitumor immune responses and have implications for the combination of radiotherapy and ICB in the clinic.

While Tumor RT promotes CD8$^+$ effector infiltration it can also increase intratumoral Tregs (Fig. 2B) and CD11b+ Gr-1^{hi} myeloid cells (Fig. 2C), which can restrain CD8$^+$ effector functions (39, 40). Our group recently demonstrated that stereotactic Tumor RT not only increases Treg intratumoral density but also enhances their suppressive function (41). Thus, the opposing immunostimulatory and tolerogenic effects of radiotherapy may provide insight into potential mechanisms to optimize synergy with immunotherapy (42). An elevated CD8 effector-to-Treg ratio has been associated with favorable prognosis and survival across multiple cancer subtypes and therefore we used this as a surrogate of favorable immune modulation in our study (15, 43, 44).

We found that increased CD8 effector intratumoral density and an increased CD8 effector-to-Treg ratio were associated with survival in our therapeutic model of stereotactic radiotherapy and ICB (Fig. 5). Among all treatment groups, Tumor RT/αCTLA4 was associated with the greatest response rate and the most favorable long-term survival outcomes (Fig. 5). We observed that the CD8 effector-to-Treg ratio was significantly increased with Tumor RT/αCTLA4 than any other regimen and therefore interrogated potential mechanisms of synergy (Fig. 6E). Anti-CTLA4–mediated Treg depletion appeared to be potentially important for combinatorial efficacy as this negated deleterious intratumoral Treg accumulation. Young and colleagues also noted a profound impact of αCTLA4-mediated Treg depletion when combined with hypofractionated radiotherapy (45). These investigators reported that combinatorial efficacy was dependent on timing of anti-CTLA4 administration as well as FcγR-dependent Treg depletion, which appears to dictate the therapeutic activity of αCTLA-4 IgG2a across several preclinical murine models (24, 35–36). We independently confirmed that αCTLA4 IgG2a appears to deplete intratumoral Tregs more efficiently than αCTLA4 IgG2b and this effect was mostly limited to intratumoral Tregs (Supplementary Fig. S5C and S5D).

Perhaps the most important observation from our studies is that ENI attenuated the synergy of stereotactic radiotherapy and αCTLA4 IgG2a. Depleting anti-CTLA4 antibodies have been demonstrated to possess dual function, potentially by promoting T-cell activation within the DLN during the priming phase and depleting intratumoral Tregs during the effector phase (24, 35–36). Our findings suggest a potentially important tolerogenic effect of ENI upon the DLN that was amplified by concurrent αCTLA4 and which promoted Treg expansion (24, 35). Curiously, αCTLA4 IgG2a combined with ENI increased the density of intratumoral Tregs, which ultimately lead to a decrease in the CD8 effector-to-Treg ratio and decrement in survival, relative to Tumor RT/αCTLA4 (Figs. 5 and 6D–E). ENI was also found to directly dampen antigen-specific antitumor immune responses. Indeed, our adoptive transfer experiments and tetramer staining revealed a significant reduction in the intratumoral density of antigen-specific functional CD8 effectors in the T+LN RT group, relative to Tumor RT (Fig. 4B). This is further corroborated by the finding that T+LN RT/αCTLA4-treated tumors were significantly less infiltrated with antigen-specific CTLs compared with Tumor RT/αCTLA4-treated counterparts. These data support the conclusion that the combinatorial effects of Tumor RT/αCTLA4 in our study results from radiotherapy-mediated antigen-specific adaptive immunity (Fig. 7A and B).

Relatively few studies to date have explored whether the combination of stereotactic radiotherapy and ICB impacts antigen-specific immunologic memory. The observation that initial treatment with radiotherapy/αCTLA4 combination regimens did confer an advantage relative to radiotherapy/αPD-1–based therapies in this model system is provocative and hypothesis-generating (Fig. 7C). While clinical data in the metastatic setting suggest that PD-1 blockade has improved efficacy and a favorable toxicity profile relative to CTLA4 blockade, it remains unknown which ICB is a more synergistic partner for stereotactic radiotherapy. Encouragingly, recent work by Twyman-Saint Victor and colleagues has demonstrated that αPD-L1, αCTLA4, and hypofractionated radiotherapy can each cooperate via nonredundant mechanisms to boost antitumor immunity (46). Consistent with our findings, De La Maza and colleagues recently showed that combination therapy with radiotherapy/αCTLA4 was superior to radiotherapy/αPD-1 in a neoadjuvant hypofractionated radiotherapy preclinical mesothelioma model (47).

In summary, our data suggest that ENI dampens adaptive immunity through perturbation of chemokine signaling leading to reduced antigen-specific immune infiltration. Furthermore, improved survival was achieved through the combination of Tumor RT that avoids the tumor-associated DLN and ICB (particularly radiotherapy/αCTLA4). Mechanistically, this combination augments the CD8 effector-to-Treg ratio and intratumoral density of antigen-specific functional CD8 effectors.

There are inherent limitations to these preclinical studies that caution broad application of these principles to clinical practice without additional investigation. Our studies were designed to explicitly evaluate localized, nonmetastatic tumors without locoregional nodal dissemination and cannot be generalized to more advanced stages of disease. Given the complex interplay between radiotherapy and immunotherapy, disease-specific, TME-intrinsic, and patient-specific factors should be taken into consideration when deciding to electively irradiate or spare the regional lymph nodes. While the mechanism of action of immunotherapy was an important determinant of response in this model, additional variables including the relative timing/sequencing of therapies, dose-fractionation schedules were not evaluated and may yield additional insight into the immunologic implications of ENI. As numerous clinical trials are underway that are actively exploring the interaction of dose/fractionation and sequencing of radiotherapy and immunotherapy, our data highlight the importance of the radiotherapy target and radiotherapy strategy. As such, this work provides

preclinical data suggesting that irradiation of the DLNs should potentially be avoided to promote combinatorial efficacy between radiotherapy and immunotherapy.

Disclosure of Potential Conflicts of Interest

A.B. Sharabi is a consultant/advisory board member for AstraZeneca. J. Wong is a consultant/advisory board member for and reports receiving commercial research grants from Xstrahl. M.J. Selby has ownership interests (including patents) at Bristol-Myers Squibb. C.G. Drake has ownership interests (including patents) in and reports receiving commercial research grants from Bristol-Myers Squibb. No potential conflicts of interest were disclosed by the other authors.

Authors' Contributions

Conception and design: A.E. Marciscano, R.A. Anders, A.B. Sharabi, D.L.J. Thorek, T.L. DeWeese, C.G. Drake

Development of methodology: A.E. Marciscano, A. Ghasemzadeh, B.J. Francica, Y. Muroyama, R.A. Anders, A.B. Sharabi, K.R. Chaudhary, D. Ulmert, D.L.J. Thorek

Acquisition of data (provided animals, acquired and managed patients, provided facilities, etc.): A.E. Marciscano, A. Ghasemzadeh, T.R. Nirschl, D. Theodros, B.J. Francica, Y. Muroyama, R.A. Anders, E. Velarde, W. Mao, K.R. Chaudhary, M.G. Chaimowitz, J. Wong, D. Ulmert, D.L.J. Thorek

Analysis and interpretation of data (e.g., statistical analysis, biostatistics, computational analysis): A.E. Marciscano, A. Ghasemzadeh, Y. Muroyama, W. Mao, T.L. DeWeese, C.G. Drake

Writing, review, and/or revision of the manuscript: A.E. Marciscano, A. Ghasemzadeh, T.R. Nirschl, D. Theodros, C.M. Kochel, Y. Muroyama, R.A. Anders, A.B. Sharabi, E. Velarde, D. Ulmert, D.L.J. Thorek, T.L. DeWeese, C.G. Drake

Administrative, technical, or material support (i.e., reporting or organizing data, constructing databases): A.E. Marciscano, C.M. Kochel, K.R. Chaudhary, J. Wong, K.B. Thudium, D.L.J. Thorek

Study supervision: A.E. Marciscano, D.L.J. Thorek

Other (provision of reagents): M. Selby

Other (provision of reagent antibodies and advised on their use): A.J. Korman

Acknowledgments

The authors thank the Experimental Irradiator Core within the Johns Hopkins Sidney Kimmel Comprehensive Cancer Center, Dr. Robert A. Anders for immunopathology expertise, the Flow Cytometry Core (Julie Nauroth) and Immune Monitoring Core (Christopher Thoburn) within the Bloomberg~Kimmel Institute for Cancer Immunotherapy as well as members of Dr. Daniel L.J. Thorek's laboratory and Dr. Jonathan D. Powell's laboratory. A.E. Marciscano was supported by an American Society for Radiation Oncology (ASTRO) Residents/Fellows in Radiation Oncology Research Seed Grant, award number 120506. A. Ghasemzadeh was supported by the NIH under award number T32GM007309. C.G. Drake was supported by NIH grants R01CA154555 and P30CA006973, the Patrick C. Walsh Prostate Cancer Research Fund, the One-in-Six Foundation, the Prostate Cancer Foundation, Melanoma Research Alliance, and the BMS International Immunotherapy Oncology Network (IIoN).

The costs of publication of this article were defrayed in part by the payment of page charges. This article must therefore be hereby marked *advertisement* in accordance with 18 U.S.C. Section 1734 solely to indicate this fact.

Received November 20, 2017; revised April 18, 2018; accepted June 8, 2018; published first June 13, 2018.

References

1. Vanpouille-Box C, Alard A, Aryankalayil MJ, Sarfraz Y, Diamond JM, Schneider RJ, et al. DNA exonuclease Trex1 regulates radiotherapy-induced tumour immunogenicity. Nat Commun 2017;8:15618.
2. Deng L, Liang H, Xu M, Yang X, Burnette B, Arina A, et al. STING-dependent cytosolic DNA sensing promotes radiation-induced type I interferon-dependent antitumor immunity in immunogenic tumors. Immunity 2014;41:843–852.
3. Harding SM, Benci JL, Irianto J, Discher DE, Minn AJ, Greenberg RA. Mitotic progression following DNA damage enables pattern recognition within micronuclei. Nature 2017;548:466–470.
4. Golden EB, Frances D, Pellicciotta I, Demaria SHelen Barcellos-Hoff M, Formenti SC. Radiation fosters dose-dependent and chemotherapy-induced immunogenic cell death. Oncoimmunology 2014;3: e28518.
5. Reits EA, Hodge JW, Herberts CA, Groothuis TA, Chakraborty M, Wansley EK, et al. Radiation modulates the peptide repertoire, enhances MHC class I expression, and induces successful antitumor immunotherapy. J Exp Med 2006;203:1259–1271.
6. Burnette BC, Liang H, Lee Y, Chlewicki L, Khodarev NN, Weichselbaum RR, et al. The efficacy of radiotherapy relies upon induction of type i interferon-dependent innate and adaptive immunity. Cancer Res 2011;71:2488–2496.
7. Fuertes MB, Kacha AK, Kline J, Woo SR, Kranz DM, Murphy KM, et al. Host type I IFN signals are required for antitumor CD8+ T cell responses through CD8{alpha}+ dendritic cells. J Exp Med 2011;208:2005–2016.
8. Dovedi SJ, Lipowska-Bhalla G, Beers SA, Cheadle EJ, Mu L, Glennie MJ, et al. Antitumor efficacy of radiation plus immunotherapy depends upon dendritic cell activation of effector CD8+ T cells. Cancer Immunol Res 2016;4:621–630.
9. Lugade AA, Moran JP, Gerber SA, Rose RC, Frelinger JG, Lord EM. Local radiation therapy of B16 melanoma tumors increases the generation of tumor antigen-specific effector cells that traffic to the tumor. J Immunol 2005;174:7516–7523.
10. Matsumura S, Wang B, Kawashima N, Braunstein S, Badura M, Cameron TO, et al. Radiation-induced CXCL16 release by breast cancer cells attracts effector T cells. J Immunol 2008;181:3099–3107.
11. Diamond MS, Kinder M, Matsushita H, Mashayekhi M, Dunn GP, Archambault JM, et al. Type I interferon is selectively required by dendritic cells for immune rejection of tumors. J Exp Med 2011;208:1989–2003.
12. Spranger S, Dai D, Horton B, Gajewski TF. Tumor-residing Batf3 dendritic cells are required for effector T cell trafficking and adoptive T cell therapy. Cancer Cell 2017;31:723.
13. Liao YP, Wang CC, Butterfield LH, Economou JS, Ribas A, Meng WS, et al. Ionizing radiation affects human MART-1 melanoma antigen processing and presentation by dendritic cells. J Immunol 2004;173:2462–2469.
14. Takeshima T, Chamoto K, Wakita D, Ohkuri T, Togashi Y, Shirato H, et al. Local radiation therapy inhibits tumor growth through the generation of tumor-specific CTL: Its potentiation by combination with Th1 cell therapy. Cancer Res 2010;70:2697–2706.
15. Sharabi AB, Nirschl CJ, Kochel CM, Nirschl TR, Francica BJ, Velarde E, et al. Stereotactic radiation therapy augments antigen-specific PD-1-mediated antitumor immune responses via cross-presentation of tumor antigen. Cancer Immunol Res 2015;3:345–355.
16. Amini A, Jones BL, Yeh N, Rusthoven CG, Armstrong H, Kavanagh BD. Survival outcomes of whole-pelvic versus prostate-only radiation therapy for high-risk prostate cancer patients with use of the national cancer data base. Int J Radiat Oncol Biol Phys 2015;93:1052–1063.
17. Blanchard P, Faivre L, Lesaunier F, Salem N, Mesgouez-Nebout N, Deniau-Alexandre E, et al. Outcome according to elective pelvic radiation therapy in patients with high-risk localized prostate cancer: A secondary analysis of the GETUG 12 phase 3 randomized trial. Int J Radiat Oncol Biol Phys 2016;94:85–92.
18. Rwigema JC, Chen AM, Wang PC, Lee JM, Garon E, Lee P. Incidental mediastinal dose does not explain low mediastinal node recurrence rates in patients with early-stage NSCLC treated with stereotactic body radiotherapy. Clin Lung Cancer 2014;15:287–293.
19. Wild AT, Herman JM, Dholakia AS, Moningi S, Lu Y, Rosati LM, et al. Lymphocyte-sparing effect of stereotactic body radiation therapy in patients with unresectable pancreatic cancer. Int J Radiat Oncol Biol Phys 2016;94:571–579.
20. Wong J, Armour E, Kazanzides P, Iordachita I, Tryggestad E, Deng H, et al. High-resolution, small animal radiation research platform with x-ray

tomographic guidance capabilities. Int J Radiat Oncol Biol Phys 2008;71: 1591–1599.
21. Jackson CM, Kochel CM, Nirschl CJ, Durham NM, Ruzevick J, Alme A, et al. Systemic tolerance mediated by melanoma brain tumors is reversible by radiotherapy and vaccination. Clin Cancer Res 2016; 22:1161–1172.
22. Li M, Davey GM, Sutherland RM, Kurts C, Lew AM, Hirst C, et al. Cell-associated ovalbumin is cross-presented much more efficiently than soluble ovalbumin in vivo. J Immunol 2001;166:6099–6103.
23. Okusanya OT, Madajewski B, Segal E, Judy BF, Venegas OG, Judy RP, et al. Small portable interchangeable imager of fluorescence for fluorescence guided surgery and research. Technol Cancer Res Treat 2015;14:213–220.
24. Selby MJ, Engelhardt JJ, Quigley M, Henning KA, Chen T, Srinivasan M, et al. Anti-CTLA-4 antibodies of IgG2a isotype enhance antitumor activity through reduction of intratumoral regulatory T cells. Cancer Immunol Res 2013;1:32–42.
25. Lauer P, Chow MY, Loessner MJ, Portnoy DA, Calendar R. Construction, characterization, and use of two listeria monocytogenes site-specific phage integration vectors. J Bacteriol 2002;184:4177–4186.
26. Rogakou EP, Pilch DR, Orr AH, Ivanova VS, Bonner WM. DNA double-stranded breaks induce histone H2AX phosphorylation on serine 139. J Biol Chem 1998;273:5858–5868.
27. Lim JY, Gerber SA, Murphy SP, Lord EM. Type I interferons induced by radiation therapy mediate recruitment and effector function of CD8(+) T cells. Cancer Immunol Immunother 2014;63:259–271.
28. Mikucki ME, Fisher DT, Matsuzaki J, Skitzki JJ, Gaulin NB, Muhitch JB, et al. Non-redundant requirement for CXCR3 signalling during tumoricidal T-cell trafficking across tumour vascular checkpoints. Nat Commun 2015;6:7458.
29. Lugade AA, Sorensen EW, Gerber SA, Moran JP, Frelinger JG, Lord EM. Radiation-induced IFN-gamma production within the tumor microenvironment influences antitumor immunity. J Immunol 2008;180:3132–3139.
30. Song X, Krelin Y, Dvorkin T, Bjorkdahl O, Segal S, Dinarello CA, et al. CD11b+/gr-1+ immature myeloid cells mediate suppression of T cells in mice bearing tumors of IL-1beta-secreting cells. J Immunol 2005;175: 8200–8208.
31. Mitsunaga S, Ikeda M, Shimizu S, Ohno I, Furuse J, Inagaki M, et al. Serum levels of IL-6 and IL-1beta can predict the efficacy of gemcitabine in patients with advanced pancreatic cancer. Br J Cancer 2013;108:2063–2069.
32. Narita Y, Kitamura H, Wakita D, Sumida K, Masuko K, Terada S, et al. The key role of IL-6-arginase cascade for inducing dendritic cell-dependent CD4(+) T cell dysfunction in tumor-bearing mice. J Immunol 2013; 190:812–820.
33. Skora AD, Douglass J, Hwang MS, Tam AJ, Blosser RL, Gabelli SB, et al. Generation of MANAbodies specific to HLA-restricted epitopes encoded by somatically mutated genes. Proc Natl Acad Sci U S A 2015;112:9967–9972.
34. Allard B, Pommey S, Smyth MJ, Stagg J. Targeting CD73 enhances the antitumor activity of anti-PD-1 and anti-CTLA-4 mAbs. Clin Cancer Res 2013;19:5626–5635.
35. Peggs KS, Quezada SA, Chambers CA, Korman AJ, Allison JP. Blockade of CTLA-4 on both effector and regulatory T cell compartments contributes to the antitumor activity of anti-CTLA-4 antibodies. J Exp Med 2009;206: 1717–1725.
36. Simpson TR, Li F, Montalvo-Ortiz W, Sepulveda MA, Bergerhoff K, Arce F, et al. Fc-dependent depletion of tumor-infiltrating regulatory T cells co-defines the efficacy of anti-CTLA-4 therapy against melanoma. J Exp Med 2013;210:1695–1710.
37. Gerber SA, Sedlacek AL, Cron KR, Murphy SP, Frelinger JG, Lord EM. IFN-gamma mediates the antitumor effects of radiation therapy in a murine colon tumor. Am J Pathol 2013;182:2345–2354.
38. Zheng W, Skowron KB, Namm JP, Burnette B, Fernandez C, Arina A, et al. Combination of radiotherapy and vaccination overcomes checkpoint blockade resistance. Oncotarget 2016;7:43039–43051.
39. Kachikwu EL, Iwamoto KS, Liao YP, DeMarco JJ, Agazaryan N, Economou JS, et al. Radiation enhances regulatory T cell representation. Int J Radiat Oncol Biol Phys 2011;81:1128–1135.
40. Xu J, Escamilla J, Mok S, David J, Priceman S, West B, et al. CSF1R signaling blockade stanches tumor-infiltrating myeloid cells and improves the efficacy of radiotherapy in prostate cancer. Cancer Res 2013;73:2782–2794.
41. Muroyama Y, Nirschl TR, Kochel CM, Lopez-Bujanda Z, Theodros D, Mao W, et al. Stereotactic radiotherapy increases functionally suppressive regulatory T cells in the tumor microenvironment. Cancer Immunol Res 2017;5:992–1004.
42. Barker HE, Paget JT, Khan AA, Harrington KJ. The tumour microenvironment after radiotherapy: Mechanisms of resistance and recurrence. Nat Rev Cancer 2015;15:409–425.
43. Sato E, Olson SH, Ahn J, Bundy B, Nishikawa H, Qian F, et al. Intraepithelial CD8+ tumor-infiltrating lymphocytes and a high CD8+/regulatory T cell ratio are associated with favorable prognosis in ovarian cancer. Proc Natl Acad Sci U S A 2005;102:18538–18543.
44. Zeng J, See AP, Phallen J, Jackson CM, Belcaid Z, Ruzevick J, , et al. et al. Anti-PD-1 blockade and stereotactic radiation produce long-term survival in mice with intracranial gliomas. Int J Radiat Oncol Biol Phys 2013;86:343–349.
45. Young KH, Baird JR, Savage T, Cottam B, Friedman D, Bambina S, et al. Optimizing timing of immunotherapy improves control of tumors by hypofractionated radiation therapy. PLoS One 2016;11:e0157164.
46. Twyman-Saints\Victor C, Rech AJ, Maity A, Rengan R, Pauken KE, Stelekati E, et al. Radiation and dual checkpoint blockade activate non-redundant immune mechanisms in cancer. Nature 2015;520:373–377.
47. De La Maza L, Wu M, Wu L, Wu L, Yun H, Zhao Y, et al. In situ vaccination after accelerated hypofractionated radiation and surgery in a mesothelioma mouse model. Clin Cancer Res 2017;23:5502–5513.